

Development of a modular hollow cathode for ground testing of plasma thrusters

Mohamed Ahmed*, Burak Karadag, Silvia Masillo, Andrea Lucca Fabris

Surrey Space Centre, University of Surrey, Guildford, GU2 7XH, United Kingdom

ARTICLE INFO

Keywords:

Electric propulsion
Hollow cathode
Modularity
Low power
Hall thruster

ABSTRACT

A hollow cathode with a modular design has been developed to assist with laboratory testing of plasma-based thrusters for satellite applications. This novel modular design includes interchangeable components for varying the geometry and tailoring the configuration to specific applications, as well as easing the replacement of individual components in the case of damage. The modular hollow cathode also presents unconventional design features aimed at improving the heating efficiency: the heater is in direct contact with the emitter and the keeper is not in physical contact with the cathode base. The modular hollow cathode development has been based on a combination of theoretical modelling and experimental testing. The influence of the novel mechanical assembly has been investigated by characterising the operational envelope at different propellant mass flow rates for xenon and krypton. The modular hollow cathode has demonstrated stable operation by sustaining discharge currents between 0.5 and 4 A at different conditions. Finally, the cathode has been coupled with a Hall-type plasma thruster operating in the 0.3–2.5 A anode current range. This paper outlines development, experimental validation of this peculiar mechanical cathode configuration, covering plasma and thermal modelling, standalone testing, and coupled Hall-type thruster operation.

1. Introduction

Hollow cathodes (HC) are key components in many plasma-based electric propulsion systems for spacecraft applications in which they provide primary electrons for sustaining propellant ionisation and ion beam neutralisation. Ongoing research on hollow cathodes in EP aims to optimise power and propellant utilisation, expand operational capabilities, and reduce complexity and costs [1]. The process of developing new hollow cathodes is often time-intensive and expensive, particularly for university EP laboratories that have limited resources and are primarily focused on research endeavours. In this article, we introduce the new design of a modular hollow cathode, intended for economical ground-based testing of electric thrusters. The modular hollow cathode features interchangeable components for easing the experimental troubleshooting and introducing flexibility in the mechanical configuration, enabling rapid updates of the device and facilitating EP prototyping. The modular hollow cathode includes a disk-shaped keeper that aids rapid ignition alongside contributing to direct heating of the emitter. This article presents the design, manufacturing, modelling and the experimental testing of the modular hollow cathode.

A zero-dimensional plasma model, previously developed at the Surrey Space Centre [2], is used to perform a numerical investigation exploring different geometrical configurations and operating regimes in

order to identify the benchmark configuration for subsequent hardware development. The results of the zero-dimensional plasma model are combined with thermal simulations using engineering software, to finalise cathode sizing, identify suitable materials, and reduce power consumption and radiative heat losses in the modular design configuration.

The modular hollow cathode is experimentally investigated at the SSC propulsion facility. The cathode is initially investigated in a standalone configuration, both in diode mode (discharge between the cathode and keeper) and in triode mode (discharge between the cathode, keeper and external anode). In diode mode, the cathode operates at different mass flow rates and the experimental results are compared to the plasma modelling outputs. In triode mode, an external positively-biased hollow cylinder is used as the anode. The keeper and anode current-voltage data are collected for two different propellant gases, xenon and krypton, within a range of mass flow rates. The discharge envelopes of the modular hollow cathode for various krypton flow rates are compared to the benchmark xenon characteristics. The choice of testing the hollow cathode with krypton has been driven by recent developments have led towards the implementation of krypton as a viable alternative propellant for Hall-thrusters [3,4].

* Corresponding author.

E-mail address: m.m.ahmed@surrey.ac.uk (M. Ahmed).

As of late 2022, due to global supply chain limitations, the price of xenon per kilogram can be approximated to almost 9000 \$/kg [5], while krypton is approximately four times cheaper than xenon. Despite being cheaper (\$/kg) than xenon, krypton's lower atomic mass and higher ionisation potential may affect system performance. However, in a Hall thruster, the lower atomic mass could increase the specific impulse by up to 25%, that could be advantageous for station-keeping satellite missions [6]. Additionally, krypton is more abundant in the atmosphere, potentially easing production [7]. Previous studies of hollow cathodes operated on krypton [6–12] showed that the higher ionisation potential increases the power requirements, and higher flow rates are needed to maintain internal pressure and emitter flux in comparison with xenon [13].

Finally, the Halo thruster [14–18], a low-power Hall effect thruster developed and manufactured by SSC, has been coupled with the modular cathode. The modular cathode and the Halo thruster have shown stable operation for more than 200 cumulative hours and the performance of the thruster has been characterised for various operating conditions [14]. Two thruster–cathode coupling configurations have been tested. In the first, the cathode is mounted externally at 45° with respect to the symmetry axis of the thruster. In the second, the cathode is centrally-mounted with respect to the thruster symmetry axis. This is done to potentially improve the coupling of the cathode plume with the thruster discharge, leading to a reduction of ion beam divergence and an improved near-field plume symmetry; moreover, the propellant supplied to the cathode is not “lost,” and contributes to the generation of thrust in the main thruster’s channel [14–16,19]. In this article, only partial results of the testing in the externally-mounted configuration are shown, since the full data set of the characterisation of the Halo thruster will be presented in a dedicated work.

This article is organised as follows. Section 2 describes the geometric architecture of the modular cathode design; Section 3 gives an overview of the transient thermal analysis and presents results of the thermal study; Section 4, provides an overview of the simulations using the in-house zero-dimensional plasma model; Section 5 presents the current–voltage characteristics for standalone configuration in both diode and triode modes, discusses the findings in comparison with the plasma model, and illustrates the results of the coupled operation with the Halo Thruster. Finally, the conclusions are presented in Section 6.

2. Modular hollow cathode design

In general, a hollow cathode comprises a refractory metal cathode tube containing an emissive insert and an externally wrapped heater, a thermal radiation shield and a keeper electrode [20]. The cathode tube frequently ends with an orifice, whose size determines the internal pressure for a given mass flow rate. The insert is a material with low work function, such as tungsten infused with barium/scandium oxide, lanthanum hexaboride, or calcium aluminate, and functions as an electron emitter [1]. The keeper electrode is a positively-biased plate that is designed with an orifice to create a potential difference for the electrons that are released from the emissive insert surface. The orifice and keeper are usually made of refractory metals as the operational temperatures can go higher than 1000 °C while maintaining a high thermal efficiency [20].

Fig. 1 compares the modular cathode to a conventional hollow cathode visually describing the novel design features. This section presents a detailed description of the laboratory model of the modular hollow cathode and the design trade-offs in comparison to conventional hollow cathodes. As illustrated in Fig. 1, the following design features apply to the modular hollow cathode:

1. The insert is in direct contact with a heating element composed of a tantalum/rhenium wire encased in boron nitride (BN) hollow cylinders. The emitter is sandwiched between a boron nitride ceramic plate and a molybdenum orifice plate. The

emitter is a tube made of barium-based compound in the pores of a tungsten matrix (BaO–W). Although lanthanum hexaboride inserts are more suitable for laboratory environments, as they are less sensitive to oxygen and water vapour in the air, BaO–W inserts are appealing due to their low work function for thermionic electron emission.

2. The keeper electrode is constituted by a molybdenum disk (positively biased), separated from the orifice plate via a ceramic spacer.
3. A polished stainless-steel tube (floating) acts as radiation shield.

The assembly is held together via mechanical fasteners without welding enabling replacement of individual components. In the case of failure, instantaneous repair or replacement of the damaged internal components can be done with limited additional manufacturing cost. The keeper electrode is used to facilitate ignition of the cathode discharge, shield the internal components from ion sputtering, and to maintain the temperature of the emissive insert or to tune the cathode performance by allowing a target current flow. In conventional hollow cathodes, the keeper has a hollow cylindrical shape with one orificed end and the other end fastened to the cathode base [1,20]. In the modular hollow cathode design, the keeper disk is not in physical contact with the cathode base, and is connected to the orifice plate using BN ceramic spacers and molybdenum fasteners. A potential issue for long-duration operations is that the sputtered molybdenum (from the keeper disk and orifice plate) may deposit on the inner surface of the hollow ceramic plate forming an electrically conductive path and causing short-circuiting between the keeper disk and the orifice plate.

The heating element comprises of three pieces of BN hollow cylinders and a refractory metal wire. The ceramic cylinders are concentrically aligned and have two rows of azimuthally-aligned holes. The refractory metal wire passes through these holes to form a zigzag line with an overall electrical resistance of 0.7 Ohm at room temperature. Fig. 2 shows a cross-section view of the modular hollow cathode. The radiation shield is 50 mm long (measuring from the keeper disk to the bottom of the ceramic base). The keeper disk measures 23 mm in diameter and 2 mm in thickness and has a 2 mm diameter hole in the centre. The ratio between the keeper orifice diameter and the orifice diameter is 2. The orifice aspect ratio is 1.

In general, the operation of hollow cathodes, particularly at low current, requires efficient thermal insulation of the emitter region. As conduction heat transfer is dominant along the cathode tube [21], a low thermal conductivity material and thin wall thickness are preferred for the cathode tube. However, manufacturing techniques and structural rigidity limit the achievable wall thickness. Feature 1 of the modular cathode attempts to promote thermionic emission and rapid ignition of the cathode discharge as the emitter is directly heated; this solution potentially reduces power consumption at the start-up and decreases conductive losses since the emitter is enclosed in ceramic elements with lower thermal conductivity.

The pressure inside the insert region of the modular hollow cathode is dependent on both the orifice diameter and the gas mass flow rate. Maintaining an internal pressure in the appropriate range is crucial for ensuring stable operation of the BaO–W emitter hollow cathode, with internal pressures typically kept below 1 mbar [22,23]. Assuming a parabolic neutral flow profile in the orifice and isothermal inviscid flow conditions as detailed in [22,23], the calculated internal pressure ranges from ~ 43 Pa (0.43 mBar) at 0.1 mg/s to ~ 215 Pa (2.15 mBar) at 0.5 mg/s. Although the internal pressure can increase during discharge, it is essential to keep it below 1 mbar to ensure the cathode’s stable performance.

In conventional hollow cathodes, the neutral gas density falls sharply in the orifice-keeper gap. As shown in Fig. 2, the modular hollow cathode uses a hollow ceramic plate (installed between the keeper disk and orifice plate) providing a relatively high neutral density. The distance between the keeper disk and the orifice is 2 mm (thickness of

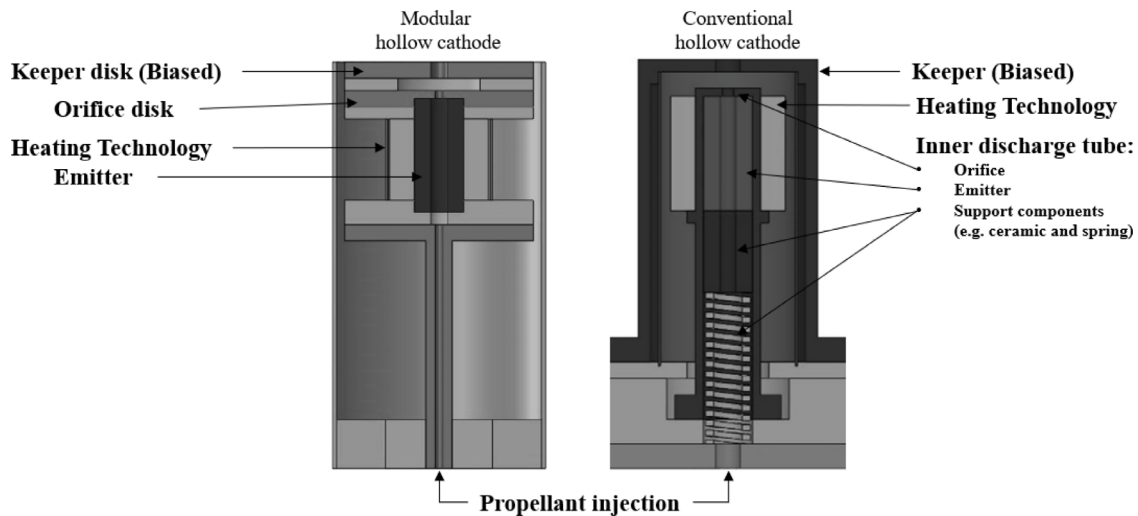


Fig. 1. A cross section view of the modular hollow cathode versus a generic hollow cathode design. On the left-hand side the novel geometric features of the modular hollow cathode and on the right-hand side conventional geometric configuration.

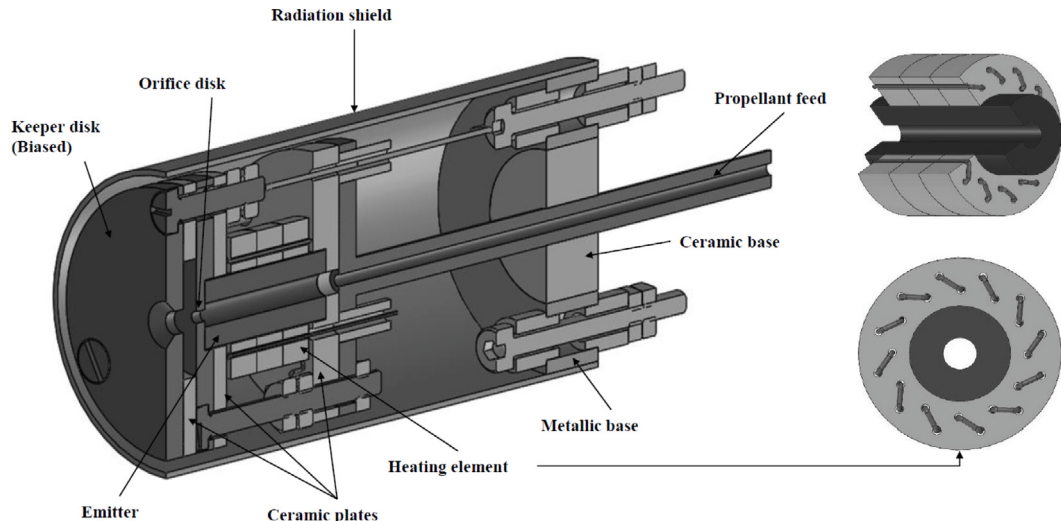


Fig. 2. A cross-section view of the modular hollow cathode with a particular focus on the heater assembly showing the zigzag configuration of the heater wire.

the ceramic), a relatively small separation distance with a small cross-sectional area (diameter of 10 mm). This feature sustains a relatively high neutral density potentially causing additional ionisation in the orifice-to-keeper gap.

During the discharge operation, the keeper electrode is heated by plasma ion bombardment [24] and/or by electrons extracted from the orifice region [25]; however, in conventional hollow cathodes this heat energy is lost to the surroundings and to the cathode base. Feature 2 is finalised to promote operation in “self-sustained” mode (heater OFF, keeper ON) for low discharge currents by forcing the heat deposited in the keeper disk to flow through the emitter before reaching the cathode base, and minimising the surface area of the keeper electrode for radiative heat loss.

3. Cathode thermal analysis: Modelling and experimental

A transient thermal study is conducted to support the material selection and validate the power budget. This thermal study uses numerical simulations to describe the thermal behaviour during the cathode ignition phase considering heating via the heater and absence of plasma. Disregarding non-linear effects such as the Schottky effect,

the Richardson–Dushman equation states that the temperature of the insert’s inner surface would need to be around 1100 °C to achieve an emission current density of approximately $5\text{--}6 \text{ A cm}^{-2}$ [1,20,26,27] that is needed for producing an electron current of 2.5 A, that is a benchmark value for the subsequent coupling with the thruster. A trade-off between the manufacturing limitations and structural properties with respect to the geometric features of the modular hollow cathode, such as wall thickness and disk length, results in the use of the selected materials with their respective thermal conductivity. In the simulations, the ambient temperature is set to 20 °C. The cathode base temperature is set to the ambient temperature which represents the cathode base temperature prior to ignition measured during experimental testing. The CAD model is simplified to reduce the computational cost of mesh generation and to facilitate the application of boundary conditions in the thermal analysis. The input loads, such as heat flow (i.e., energy addition over time) and radiative component (i.e., surface thermal radiation), are used as boundary conditions in the model. These loads are simulated over constant step controls within the model. The material properties used in the model are reported in Table 1. The emissivity of the emitter is not considered and convective heat transfer with the neutral gas flow in the insert is also neglected, therefore heat

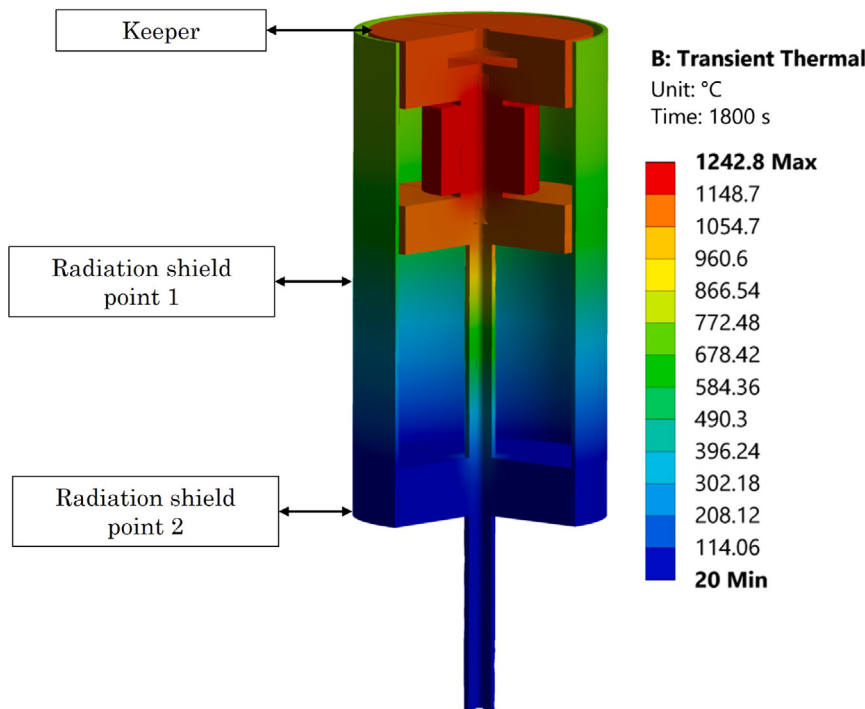


Fig. 3. Sectional view of the thermal simulations based on material properties and geometry at 130 W heating power for the selected material properties described in [Table 1](#). The output in the transient state takes into consideration the behaviour that varies over time. Besides thermal conductivity, the specific heat and density of each material are also specified in the material properties of the model.

Table 1
Material thermal properties.

Materials	Emissivity [27] [28]	Thermal conductivity at room temperature [W m ⁻¹ C ⁻¹]
Molybdenum	0.1	120
Boron nitride	0.8–0.9	49.96
Stainless steel	0.2–0.3	30
Barium oxide impregnated with Tungsten	–	70

is transferred by conduction and radiation only. Surfaces in contact with each other are assumed to be bonded to allow for perfect thermal contact conductance, i.e., no thermal contact resistance is applied. The influence of the support structure on the cathode assembly is disregarded. In the thermal model, the changes in thermal conductivity and emissivity with increase in temperature are not implemented.

The thermal model output is shown in [Fig. 3](#). To assess the validity of the simulations and to evaluate the thermal behaviour of the cathode during the ignition process, an experimental investigation with solely heating power (i.e., without plasma discharge) has been performed. The predicted results at the keeper disk and at the mid-point of the radiation shield are compared to the experimentally measured results during a heating period of 30 min showing similar trends with an approximately 35% offset of the temperature. Measurements of the temperature variation at three distinct points, including the keeper plate, the midpoint of the radiation shield (Radiation shield point 1), and the end of the radiation shield (Radiation shield point 2), are obtained using K-type thermocouples as shown in [Figs. 3 and 4](#). The investigation is conducted for a period of 30 min at operational heater powers ranging from 0 to 130 W. The heater power supply operates in current control (CC) mode and initially set to 5 A. Over the following 5 min, an increase in temperature, reaching over 450 °C at the keeper plate and 150 °C at Radiation shield point 1, is recorded for a heater

power of approximately 50 W. Subsequently, the heater current is increased by 1 A causing an immediate increase of the temperature to 480 °C at the keeper plate and 200 °C at the Radiation shield point 1 for a heater power of approximately 75 W. The heater is kept at a 6 A current for a duration of 10 min recording 600 °C at the keeper plate and 300 °C at the Radiation shield point 1 at the end of this phase. The temperature increase results in an increase in resistance and, therefore, power as the heater operates current control mode. Subsequently, the heater current is increased to 7 A with a heater power of 110 W causing a keeper plate temperature of 670 °C and of 370 °C at Radiation shield point 1. Finally, the heater current is set to 7.5 A for an additional 5 min recording approximately 750 °C at the keeper plate, 430 °C at the Radiation shield point 1, and 400 °C at the Radiation shield point 2 for a heater power of approximately 130 W. An additional attempt to increase the current further has unexpectedly caused a drop in power. This anomaly could be due to a change of thermal conductivity and electrical resistivity of the materials as the change in power is transient with an increase in heater current.

The plots in [Figs. 5 and 6](#) compare the temperature as a function of the heater input power for the experimental results versus the simulation outputs. There are two important uncertainty sources: 1) the emissivity of the cathode surfaces can significantly differ from the nominal values due to changes of the surface properties as a result of plasma exposure; 2) the unaccounted thermal contact resistance. A factor that can potentially justify the offset between experimental and simulated results is the fact that the modular cathode accumulated tens of ignition cycles prior to the thermal management study, causing changes in the surface properties of the assembly, in particular of the radiation shield and the keeper disk. The key mechanism of heat transfer from these two elements is via radiation. As an example, a coating is observed on the stainless steel radiation shield which can alter the emissivity. In addition, as the operating temperature increases the thermal conductivity varies. As an example, the molybdenum parts have a low surface emissivity of approximately 0.1 and thermal conductivity of molybdenum decreases as the temperature increases making

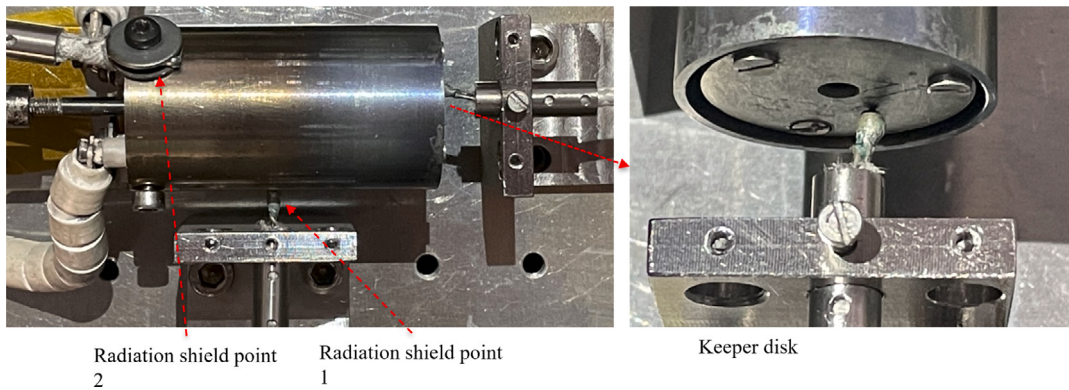


Fig. 4. Temperature study set-up.

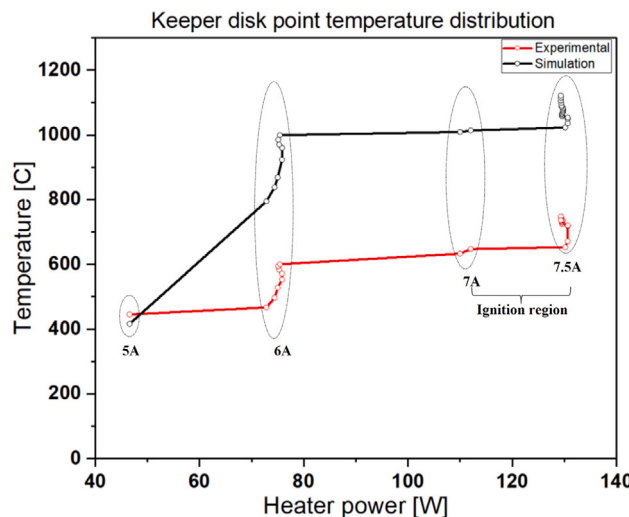


Fig. 5. Transient thermal model output versus experimental results at the keeper disk.

molybdenum a favourable choice as heat losses need to be drastically reduced [27,29]. In comparison to the predicted results seen in Fig. 3, the experimental time to reach a steady state condition is longer owing to non-ideal joints. However, the thermal characterisation experiment confirms that the cathode can sustain the required emission parameters, temperature and current for a heating power in the 110–130 W range.

4. Zero-dimensional plasma model simulations

Previous studies have demonstrated acceptable agreement between zero-dimensional plasma modelling and experimental data [30–33]. The zero-dimensional plasma model provides quantitative predictions of the power deposition within the insert and orifice regions for varying geometrical and operational boundary conditions. The model is effective for developing conventional hollow cathodes incorporating thermionic emitters. The model offers information on the power of the discharge, how the power is distributed across the plasma regions, and the amount of power deposited on the internal walls. Using iterative methods where plasma properties are averaged, the plasma model solves conservation equations for mass, current, and power in two distinct areas — the insert and orifice regions. A full description of the model, including its core equations and computational sequence as well as a preliminary validation with respect to experimental data, is provided in [2]; here, we report a general overview and a summary of

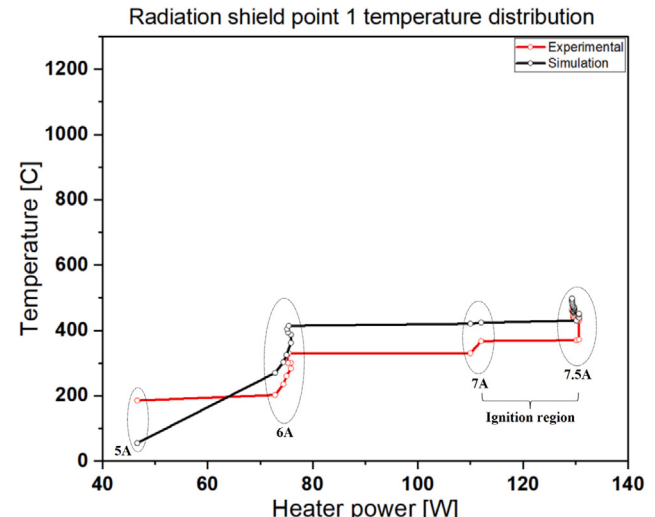


Fig. 6. Transient thermal model output versus experimental results at the Radiation shield point 1.

the key features. This model was previously exploited in a conventional hollow cathode neutraliser development at SSC. The model computes various plasma characteristics such as the plasma density, electron temperature, and sheath potential. The wall temperature is considered an input parameter that can either be manually selected or linked to a separate thermal model. The model assumes that the plasma comprises three species, namely, neutrals, electrons, and singly-charged ions. In addition, for simplicity, the length of the plasma discharge (i.e., the attachment length) is equal to the total length of the insert and the temperature gradient of the emitter is neglected. The Poiseuille law is used to govern the neutral flow, and the flow through the orifice region is considered as choked. The work function of the BaO-W411 used is 1.67 eV with a Richardson constant of $120 \text{ A cm}^{-2} \text{ }^{\circ}\text{C}^{-1}$ [20,34]. The wall current balance involves various mechanisms that contribute to the discharge behaviour, including thermionic emission, as well as internal ion and electron fluxes towards both the insert and other nearby collecting surfaces.

The cathode internal plasma volume is divided into two cylindrical regions, one enclosed within the hollow insert and delimited by four boundaries, and the other containing the orifice delimited by three boundaries. Fig. 7 illustrates the insert region on the left and the orifice region on the right. The plasma boundary between the insert and orifice regions is a double sheath that forms due to the continuity of the

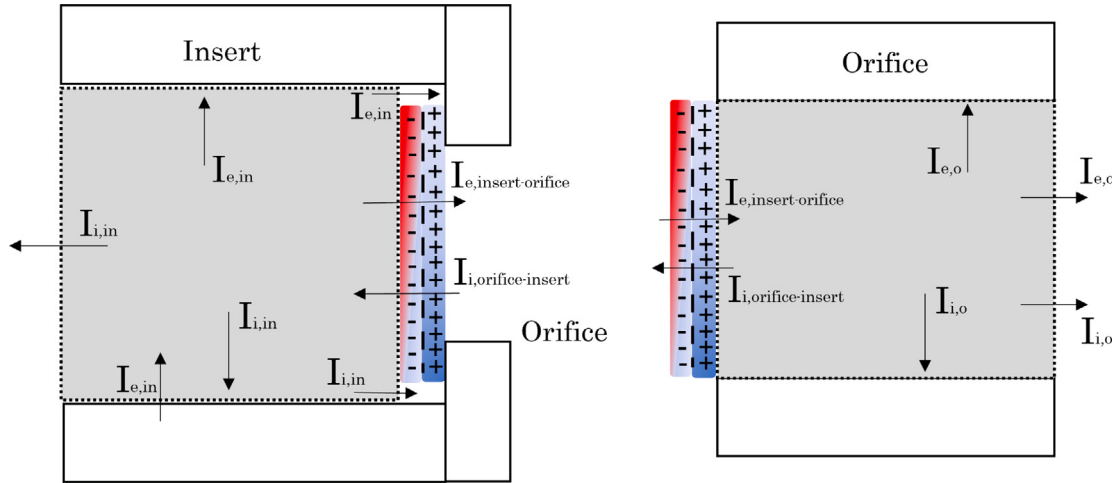


Fig. 7. Illustration of the simulation regions.

discharge current. To ensure a consistent discharge current through the bottleneck region, the orifice region presents a higher electron density relative to the insert region [2,35]. A boundary, known as the double sheath, forms where the insert region has a net negative charge and the orifice region has a net positive charge. This configuration permits the transfer of electrons from the insert to the orifice region while bouncing back any electrons that originate from the orifice region, i.e., the double sheath serves as a barrier that permits the transfer of electrons from the insert to the orifice while blocking their movement in the opposite direction. The same applies to ions, which can pass through the double sheath when coming from the orifice region but are repelled back if originating from the insert side. Furthermore, the orifice plasma volume permits the departure of both ions and electrons through the downstream and lateral walls of the orifice [2]. The model for the insert region has four boundaries that enclose the region: the orifice plate and double sheath on the right, the upstream boundary on the left, and the thermionic emitter on the lateral side. The upstream boundary only permits ion outflow from the insert region, while electrons from thermionic sources enter the plasma via the lateral boundary by crossing the plasma sheath potential. The walls of both the insert and orifice regions are conductive and have the same potential in the plasma sheath. The Richardson–Dushman equation and the Schottky effect equation are employed to model the thermionic current.

The performance of the hollow cathode is observed by computing the voltage, current, and discharge power. The model also predicts the power deposition on the emitter and orifice surface due to ion and electron bombardment. An external thermal model can be used to calculate the temperatures of the insert and orifice walls using the power deposited by ion and electron impacts on the internal surfaces as inputs. The plasma model focuses on the insert and orifice regions but disregards the keeper sheath and the cathode-to-keeper region. Therefore, the overall power calculated by this model does not account for the cathode-to-keeper region. More details on the zero-dimensional plasma model can be found in [2,36]. In this previous article, the model's response to changes in the cathode's geometrical and operational conditions was quantitatively analysed, and the numerical results were found to be in agreement with experimental data reported in the literature. The results of the simulations support the analysis of the feasibility of the geometrical configuration of the emitter and the orifice of the modular hollow cathode.

According to the investigation using the thermal model detailed in Section 3, the estimated operating temperature of the insert is approximately between 1050 and 1240 °C. The thermal model has been validated independently from the zero-dimensional plasma model.

Table 2
Geometrical dimensions and operating conditions of the modular hollow cathode.

Parameters	
Orifice diameter [mm]	1
Orifice length [mm]	1
Insert diameter [mm]	2
Insert length [mm]	14
Insert temperature ($T_{w,in}$) [°C]	1070
Discharge current [A]	1.5
Insert material work function [V]	$1.67 + 2.82 \times 10^{-4} T_{w,in}$
Xenon mass flow rate [mg/s]	0.1–0.3

While there is a close correlation between the discharge current and insert temperature, the plasma model has not been integrated with the thermal model yet. Hence, the primary focus is on the overall trend of the results rather than the precise relationship between discharge current and insert temperature.

The plasma model results obtained for the modular hollow cathode are here presented and discussed. The key geometric and operational parameters considered in the simulations are provided in Table 2. The power distribution components, including the power required to accelerate emitted electrons through the sheath (P_s), the resistive heating power in the insert region ($P_{Q_{\text{insert}}}$) and orifice region ($P_{Q_{\text{orifice}}}$), and the double sheath power necessary for electron and ion acceleration at the interface between the insert region and orifice region (P_{ds}), are illustrated in Figs. 8 and 9. These figures demonstrate how the power distribution changes depending on the discharge current value. According to the model, when the discharge current increases, the proportion of joule heating in the orifice region increases while the proportion of power in the insert region decreases. Nevertheless, all power components exhibit an increase in absolute values with an increase in discharge current. This examination indicates that the power utilised in accelerating ions and electrons through the double sheath in the orifice region rises both in terms of proportion and actual amount. The reason for this can be attributed to the fact that the power transferred through the double sheath is dependent on the electron temperature, electron density, and orifice cross-sectional area.

Fig. 10 depicts the effect of mass flow rate on the power distribution for the modular cathode geometric configuration, considering a discharge current of 1.5 A. The zero-dimensional plasma model predicts that increasing the mass flow rate results in a reduction in both overall discharge power and joule heating. In the orifice region, the electron density shows a higher rate of increase for increasing flow rates than that of the insert region, which remains relatively constant throughout

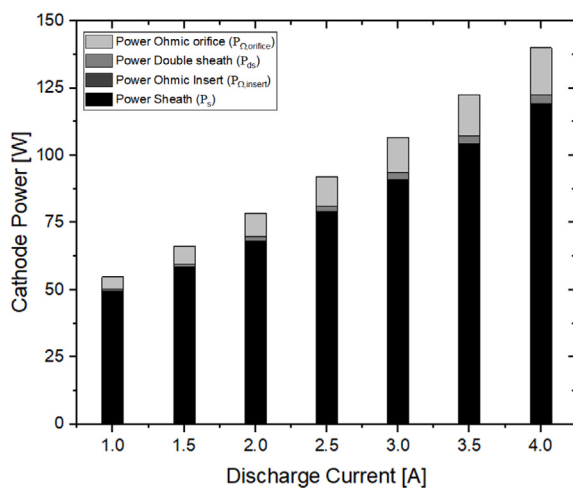


Fig. 8. Power breakdown as a function of the discharge current at 0.1 mg/s of xenon. The model inputs are in Table 2.

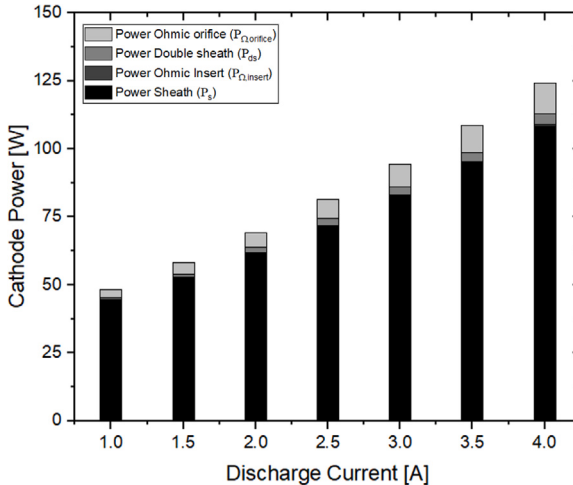


Fig. 9. Power breakdown as a function of the discharge current at 0.3 mg/s of xenon. The model inputs are in Table 2.

Table 3
Power budget of the modular hollow cathode for the operational conditions listed in Table 2.

Discharge current [A]	1.5	
Mass flow rate [mg/s]	0.1	0.3
Total input power [W]	67.9	60.0
Discharge power [W]	66.3	58.4
Power transported by extracted electrons and ions [W]	14.5	10.9
Power re-deposited into the cathode [W]	53.4	49.1

Table 4
Ignition specifications.

Heater ignition power [W]	110–130
Keeper ignition voltage [V]	200–250
Ignition mass flow rate [mg/s]	0.2
Discharge current [A]	0.5–4
Operating mass flow rate [mg/s]	0.1–0.3
Cathode mass [g]	105

the range of mass flow rates studied (see Fig. 11). Furthermore, as shown in Fig. 12, a rise in xenon mass flow rate from 0.1 mg/s (1 sccm) to 0.3 mg/s (3 sccm) causes a steeper decrease in electron temperature in the orifice region than in the insert region, where it remains relatively constant.

The modular hollow cathode's total input power, discharge power, and power deposition at different mass flow rates are presented in Table 3. The table provides the power components of the ions and electrons extracted through the cathode orifice, as well as the remaining power re-deposited on the internal surfaces within the system.

5. Cathode discharge experimental characterisation and discussion

5.1. Experimental setup for standalone testing

The standalone experiments are performed in the Dinko vacuum chamber at the SSC propulsion laboratory, University of Surrey. The vacuum chamber measures 45 cm in diameter and 50 cm in length and has a two-stage pumping system, which consists of a roughing pump and a turbo-molecular pump. The vacuum chamber achieves a base pressure in the range of 10^{-6} mbar without mass flow rate. It is equipped with a variety of feedthroughs, propellant feedlines, cathode power lines, a viewing port, and a pressure gauge to measure pressure levels in the chamber. The current pumping system of the vacuum chamber has a nominal pumping capacity of 300 L/s for nitrogen.

The cathode return is electrically connected to the vacuum chamber wall (the ground reference of the system) for diode operation, whereas it is floating in the case of triode mode testing and a voltmeter is incorporated in the line for cathode-to-ground voltage measurement. This latter configuration reproduces a standard thruster testing setup. The modular cathode is powered by three power supplies. The heater is controlled using an Aim-TTi CPX200DP (0 to 60 V and 0 to 20 A) power supply. The keeper is controlled using Sorensen 1.2 kW Programmable DC Power Supply, (0–300 V and up to 4 A). In triode mode, the anode current is controlled using an Aim-TTi CPX200DP (0 V to 60 V and 0 A to 20 A) power supply. The keeper and anode power supplies share a common ground and the mounting interface of the cathode is electrically floating.

Fig. 13 shows a schematic of the experimental setup including the vacuum chamber system, neutral gas feed system and power supplies. The mass flow controller is an MKS 1179C 2 mg/s controller with a 4 channels flow controller power supply readout unit (TYPE 247D). This controller is calibrated for xenon. In Fig. 14, the modular hollow cathode assembly is seen with and without the radiation shield.

5.2. Ignition characteristics and operational envelope

The presentation of the modular cathode's discharge characteristics has been divided into two sections, describing diode mode and triode mode operation respectively. In both modes, the discharge voltage and discharge current are characterised at varying mass flow rates for xenon and krypton (the latter used in triode mode only). In triode mode, the cathode–anode distance is fixed at 30 mm. The ignition is successful and repeatable at a heating power of 130 W and few seconds after ignition, the heater power supply unit is turned off and the cathode operates in “self-sustained” operation (heater OFF, keeper ON). A summary of the ignition characteristics and operational envelope for the different experimental campaigns can be seen in Tables 4 and 5, respectively. The background pressures are corrected for xenon and krypton.

Table 5
Experimental operational characterisation summary.

Test configuration	Propellant	Mass flow rate [mg/s]	Chamber pressure [mbar]	Keeper current [A]	Anode current [A]
Standalone	Diode	Xe	0.1–0.3	6.6E–5–1.6E–4	1–4
	Triode	Xe	0.1–0.3	6.6E–5–2.2E–4	1, 1.5, 3
		Kr	0.1–0.3	9.8E–5–2.8E–4	1.5, 3
Coupled with Halo Thruster		Xe	0.1	9.2E–6–1.5E–5	2.5
					0 – 2.5

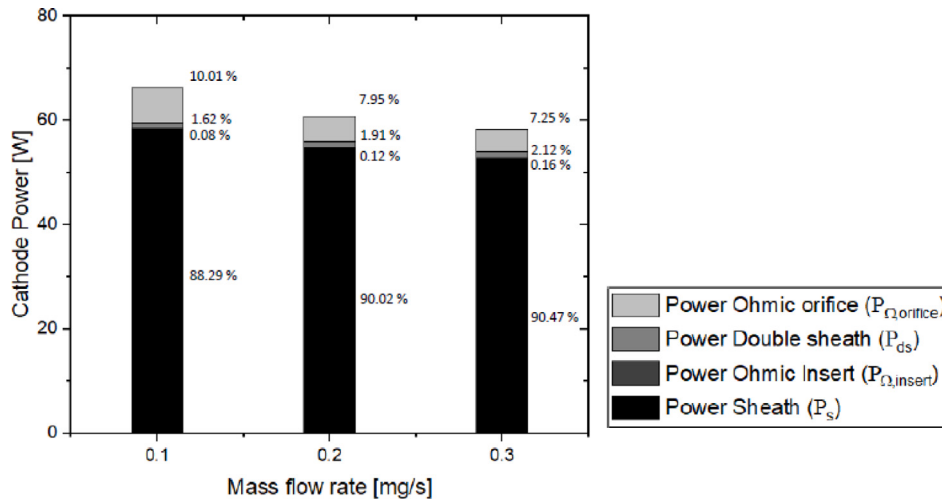


Fig. 10. Power distribution breakdown as a function of mass flow rate for a discharge current of 1.5 A. The operational condition are shown in Table 2.

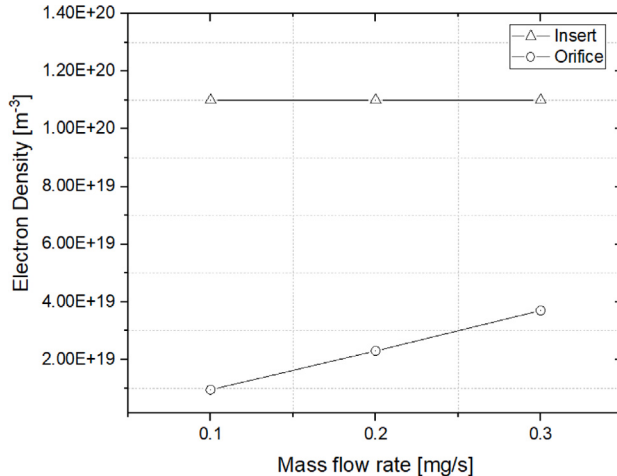


Fig. 11. Electron density as a function of mass flow rate for discharge current of 1.5 A.

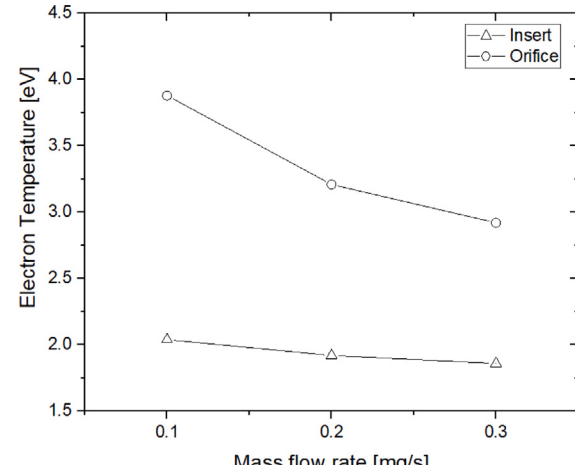


Fig. 12. Electron temperature as a function of mass flow rate for discharge current of 1.5 A.

5.3. Diode mode operation

In diode mode, the modular cathode is characterised using an ignition procedure that involves applying a voltage of 250 V to the keeper and a mass flow rate of 0.2 mg/s. To avoid excessive keeper current, the keeper current is limited to 3 A during ignition. Once ignition is achieved, the flow rate is set to the target mass flow rate and the keeper operates in current control mode. In Fig. 15(b), cathode operation at 0.1 mg/s and discharge current of 1.5 A is seen. Fig. 16(a), illustrates the operational voltage for various flow rates as a function of discharge current, resulting from the experimental testing. Each data point represents the mean of five repetitions and the error bar is evaluated at the respective standard deviation. For all the mass flow

rates, the profiles show that as the discharge current decreases, the discharge voltage of the keeper increases.

The keeper voltage is expected to be greater than the plasma voltage in the internal plasma region. This elevated keeper voltage serves to uphold a quasi-neutral state in the emitter region and reduce ion energy at the emitter [20,22,37,38]. Additionally, the zero-dimensional plasma model computes a constant electron temperature at the emitter region as the discharge current is swept from 1 to 4 A for all the selected mass flow rates.

Fig. 16(b) shows a comparison between the predicted voltage envelope at different mass flow rates and discharge currents resulting from the plasma model simulations and experimental data obtained for the modular hollow cathode. The comparison reveals a good agreement

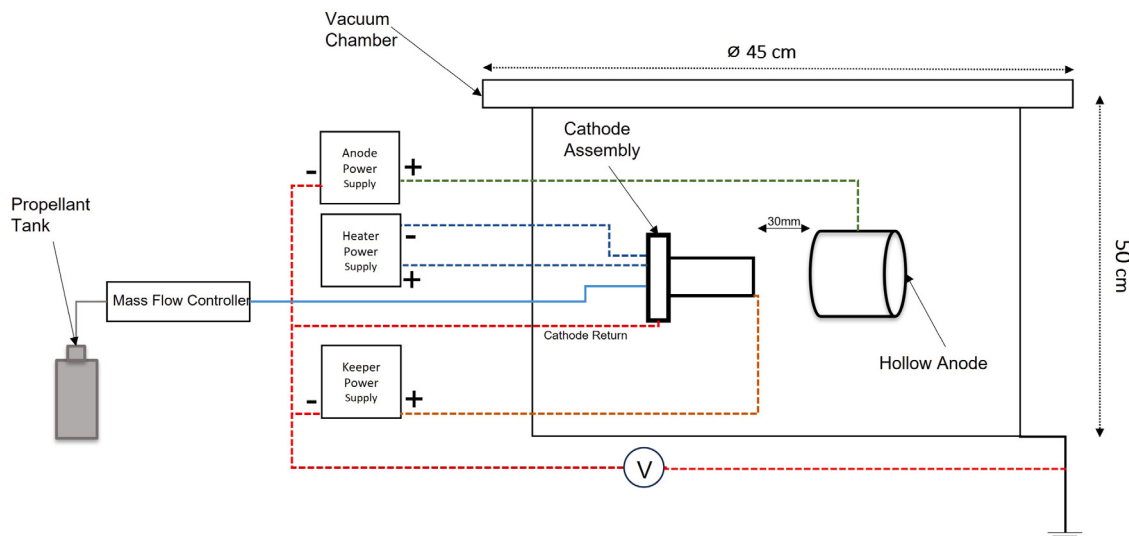


Fig. 13. Experimental setup for the characterisation of the modular hollow cathode.



Fig. 14. Modular hollow cathode assembly. On the left: The internal skeleton of the cathode assembly without the radiation shield and not secured fasteners. On the right: The complete assembly including the radiation shield.

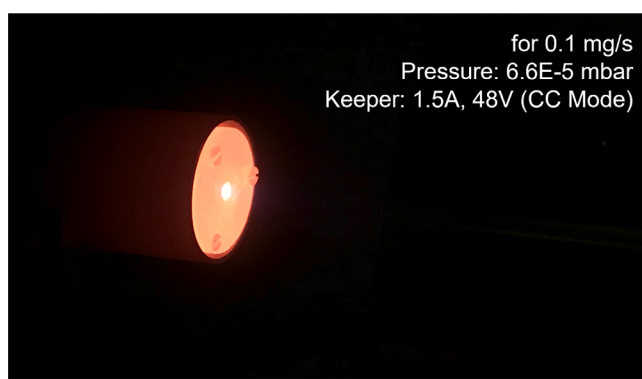


Fig. 15. Diode mode operation at 1.5 A at 0.1 mg/s mass flow rate.

between the experimental and modelled results, with a discrepancy of less than 20%. It is important to note, however, that the modelled discharge voltage considers only the voltage drop up to the cathode orifice and does not consider the voltage drop in the cathode-to-keeper

region. This factor, along with inherent assumptions at the basis of the model and experimental measurement uncertainties, all contribute to the discrepancy seen in Fig. 16(b).

5.4. Triode mode operation

The modular cathode is coupled to an auxiliary positively-biased electrode (a 50 mm diameter hollow cylinder) positioned 30 mm away from the keeper. The ignition procedure uses a mass flow of 0.2 mg/s, and a voltage of 250 V to the keeper. The keeper current is limited to 3 A. After ignition, the flow rate is set to the target mass flow rate, and a voltage of 50 V is applied to the anode. The keeper and anode currents are subsequently set to their target values via current control operation. In the figures presenting the results of this study error bars are not included to allow for visibility of the trends, nevertheless each data point reported in the figures is the mean of 6 repetitions. The lowest anode current investigated for this new geometry is 0.5 A and the highest is 3.5 A. Attempts to operate at 4 A results in discharge instability. In Fig. 17, the modular hollow cathode operation in triode mode is seen.

The influence of the keeper current for fixed values of the mass flow rate and of the auxiliary anode current is investigated, with keeper currents of 1, 1.5 and 3 A at 0.1 mg/s. This study is illustrated in

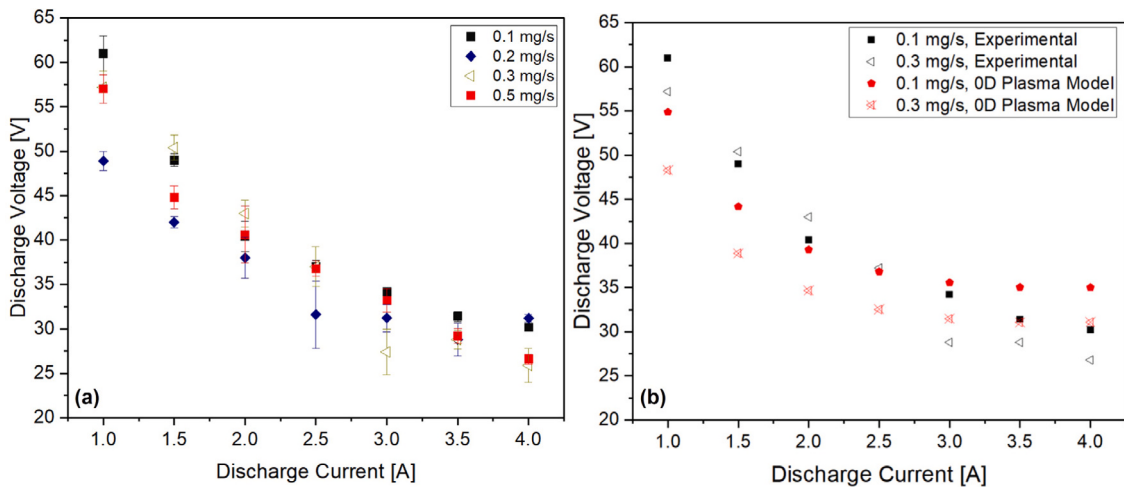


Fig. 16. (a) Experimental diode mode operation on xenon for different mass flow rates. (b) Zero-dimensional plasma model versus experimental operation in diode mode at 0.1 and 0.3 mg/s of xenon.

Fig. 18. Operation at low mass flow results in lower plasma density and higher plasma resistivity; this increases the sheath potential resulting in high electron energies. At a higher keeper current, the anode voltage-current profile is approximately flat translating to a constant discharge impedance as seen in Fig. 18. However, at low keeper currents, the anode voltage decreases for increasing anode currents indicating a negative discharge impedance.

The keeper voltage decreases with an increase of the keeper current for a constant anode current. The increase in keeper power deposition improves the total emission current by adding extra heating, as seen in Fig. 19. An increase in keeper current increases the electron current density. This, in turn, leads to a higher plasma density and higher electron temperature, and generates additional joule heating. In addition, the insert temperature has a direct effect on the electron current generated. This can potentially be a problem at low discharge currents because the emitter temperature decreases. However, the thermal distribution of the modular hollow cathode can potentially sustain the necessary emission temperatures at lower discharge currents based on heat deposition from the plasma into the emitter.

The influence of the mass flow rate on anode and keeper voltages is characterised as a function of the auxiliary anode current for a fixed keeper current. The keeper voltage decreases with an increase in the anode current and is approximately independent on the mass flow rate implying a constant keeper power, as shown in Fig. 20. The anode voltage for a certain anode current decreases with an increase in the mass flow rate as seen in Fig. 20. The anode potential does not show significant temporal anomalies over timescale of seconds at constant keeper/anode currents during this study (only timescales of seconds have been considered and higher frequency oscillations have not been monitored). In addition, as the anode current and mass flow rate are swept, the cathode-to-ground voltage varies from -13.5 to -0.5 V. The magnitude of the cathode-to-ground voltage increases as the anode current increases at various flow rates. During the study in triode mode, the cathode is observed to switch between spot and plume operation, which are modes of operation for which the names derive from the visual appearance of the cathode external discharge.

In the triode mode of operation, the modular cathode is observed to operate either in spot or plume mode when the current and flow rate are varied. However, a full characterisation of these transitions is not the focus of this study. In general, the spot mode features a “spotlike” discharge at the orifice and a dark anode space from visual observations. The transition from spot mode to plume mode occurs when the plasma density at the orifice of the cathode is below a certain threshold [8] which is necessary to sustain the target current from the

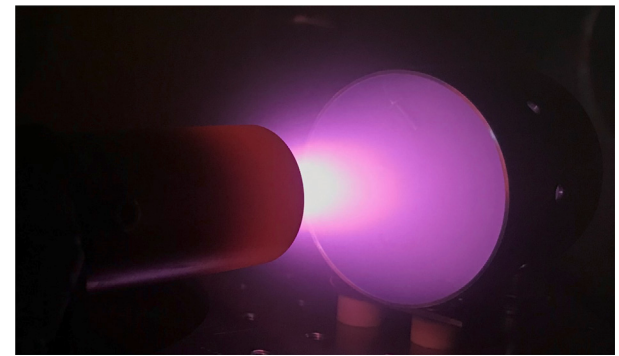


Fig. 17. Modular Hollow Cathode operation in triode mode. The external anode is visible in front of the cathode.

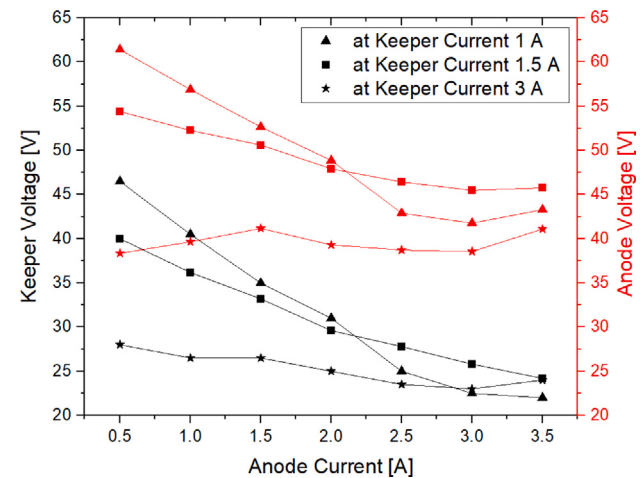


Fig. 18. Effects of anode current and keeper current in the triode operational mode on 0.1 mg/s of xenon.

downstream quasi-neutral plasma. At lower mass flow rates and/or higher anode currents, the plasma density may not be high enough to sustain the spot mode operation, and the discharge may become unstable and transition to the plume mode. The plume brightness and divergence increases with an increase in collecting potentials is noted.

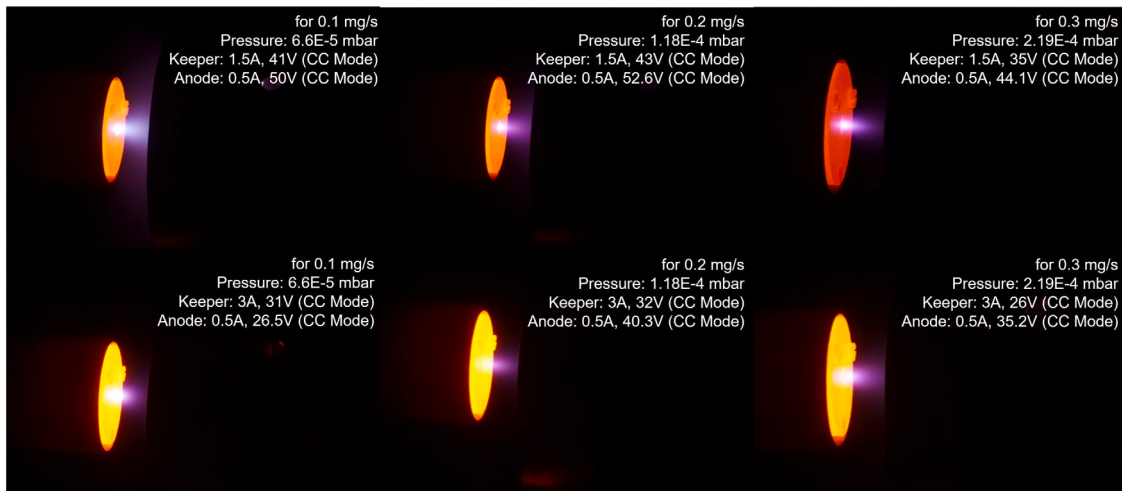


Fig. 19. Effects of the keeper current at different mass flow rates during triode mode operation. The exposure time for all the images is not the same.

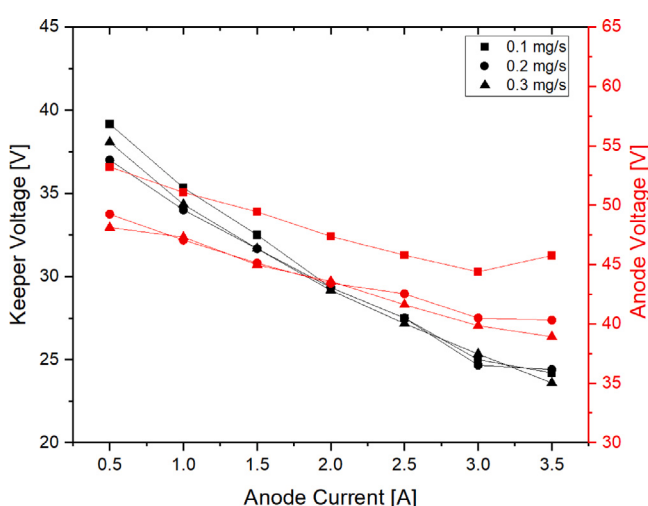


Fig. 20. Effects of the mass flow rate in the triode operational mode on xenon. The keeper current is 1.5 A.

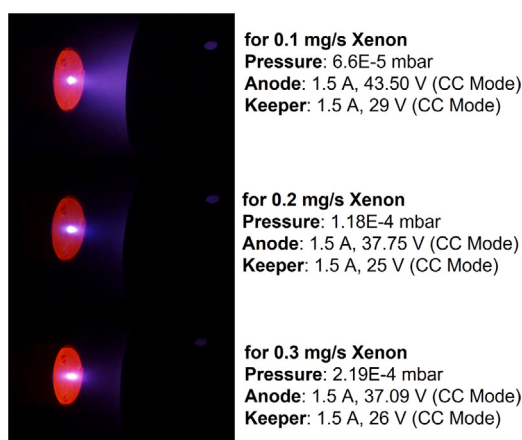


Fig. 21. Operation at different mass flow rate during the triode mode characterisation. The exposure time for all the images is the same.

According to previous studies [22,39,40], cathode-to-anode distance, operational mass flow rate, discharge current, and background pressure influence the mode of operation. The transitional behaviour of the modular hollow cathode as a function of xenon mass flow rate is visually observed in the images of the discharge plume of Fig. 21. Previous findings that hollow cathodes switch from spot mode to plume mode operation as the mass flow rate is reduced [8,41,42], are supportive of this conjecture.

A second characterisation campaign is carried out using krypton, a low cost viable alternative propellant for electric propulsion systems as demonstrated by recent developments [3]. The campaign aims to investigate the performance of the modular hollow cathode on krypton. After ignition, the keeper and the anode operate in current control mode. The collected data is based on the mean of 3 repetitions. Fig. 22 presents the triode mode results for various krypton mass flow rates (0.1 mg/s, 0.2 mg/s, 0.3 mg/s) and keeper current values of 1.5 and 3 A as the anode current is swept between 0.5 and 3.5 A replicating the xenon experimental campaign. However, the discharge is unstable at 3.5 A at the selected operational flow rates. The ignition uses a heating power of 130 W with a constant mass flow rate of 0.2 mg/s. The keeper potential is set to 250 V with the current limited to 3 A. After ignition, the cathode operates in self-sustained mode (heater OFF, keeper ON). In addition, as the anode current and mass flow rate are swept the cathode-to-ground voltage varies from -8.7 to -3.2 V.

The discharge characteristics of the modular hollow cathode are presented in Fig. 22. At a constant keeper current of 1.5 A and a mass flow rate of 0.1 mg/s, the anode voltage ranges between 46.6 V to 44.4 V. Initially, the anode voltage increases, but as the anode current is further increased, it decreases. A similar trend is observed at higher mass flow rates of 0.2 and 0.3 mg/s, where the anode voltage decreases with an increase in anode current up to 2 A, followed by a flat profile. At a higher keeper current of 3 A, the anode voltage ranges from 23.1 to 42.6 V. The anode voltage presents an initial ramp as the anode current is increased to 1.5 A and reaches a plateau for higher anode currents, determining a constant discharge impedance. These trends are consistent across all mass flow rates as shown in Fig. 22. In Fig. 23, the performance of the modular hollow cathode operation on krypton at 0.1 mg/s and 0.2 mg/s is compared with that observed with xenon, showing similar voltage-current trends for both anode and keeper. As the anode current is increased for a constant keeper current, in general the anode potential decreases for both cases of xenon and krypton operation. However, the following tendencies have been noted. Firstly, at 0.1 mg/s of krypton and 0.5 A anode current, a reduced anode voltage is observed indicating a lower voltage difference needed for

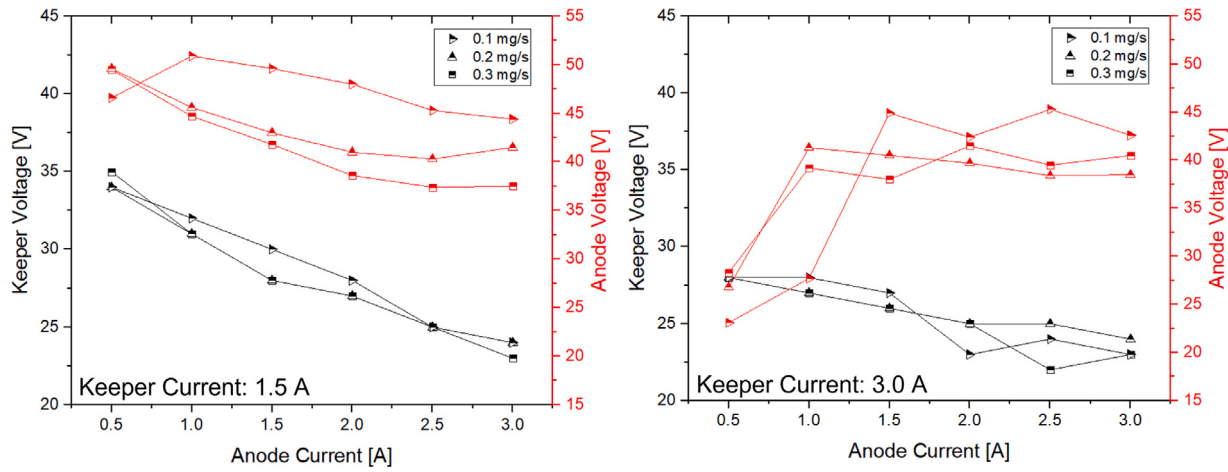


Fig. 22. Triode operational mode on krypton at keeper currents of 1.5 A (on the left) and 3 A (on the right) for mass flow rates of 0.1, 0.2 and 0.3 mg/s.

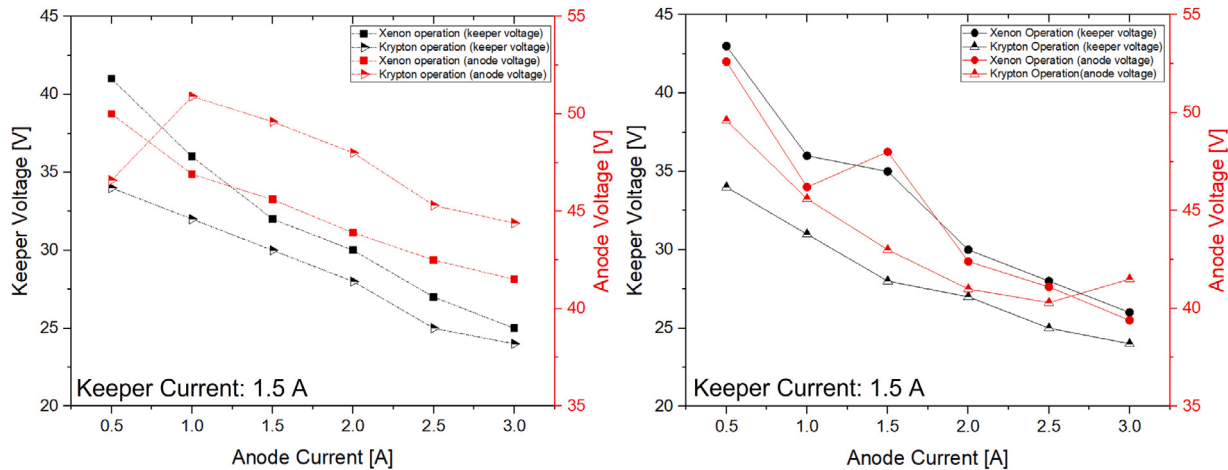


Fig. 23. Triode mode operational comparison at 1.5 A keeper current between 0.1 (left) and 0.2 (right) mg/s of xenon and krypton.

extracting the same electron current. Secondly, at 0.2 mg/s of krypton, as the anode current is swept, the anode voltage is lower in comparison to xenon; indicative of a different mode of operation at this flow rate. A lower divergence of the plume is also observed in the case with krypton. Nevertheless, this study is focused on identifying and characterising the current–voltage envelope of the modular cathode and the effects of the anode and keeper voltages on the plume properties for xenon and krypton have not been investigated. The cathode discharge power (sum of keeper and anode power) required is higher for krypton, as depicted in Fig. 24, which reports the cathode discharge power as a function of the mass flow rate at different keeper and anode currents. At 0.2 mg/s and anode current of 1.5 A, a spurious fluctuation in the keeper and anode voltage on xenon is observed, resulting in higher cathode discharge power at that operating condition.

5.5. Coupling with a Hall effect-based thruster

The cathode is coupled with the Halo thruster, a low-power Hall effect-based thruster developed at the SSC [15–17]. The Halo thruster features a cusped magnetic field with magnetic cancellation regions and a cylindrical discharge channel, and produces a thrust level between 6 and 15 mN with a specific impulse of 550–1100 s [16,17]. The coupled system is tested at power levels below 1 kW. The results presented in this section are for the case with the externally-mounted modular hollow cathode with an angle of 45° with respect to the symmetry axis

of the thruster. The modular cathode coupled with the Halo thruster can be seen in Fig. 25. The cathode position and operational parameters influence the performance of the thruster [19,43–45], affecting both the cross-field discharge behaviour and the plume characteristics. The potential drop between the anode and the cathode generates the electric field needed for accelerating the ions. In order to ignite the cathode, a heating power of 130 W is gradually applied over the benchmark heating period described in Section 3. Once ignited, the keeper current is set to 2.5 A, the cathode flow rate to 0.1 mg/s in self-sustained mode (heater OFF, keeper ON). The anode voltage is swept between 150–350 V at 20 V steps in order to examine the discharge characteristics and operational stability. The tests are performed in the Deadulus vacuum chamber at the SSC propulsion lab. Details on the facility can be found in [15]. Fig. 26 illustrates different thruster parameters for constant self-sustain cathode operation. The cathode-to-ground voltage for this operational range varies from -91.7 V to -40 V for anode mass flow rates of 0.98, 1.47 and 1.96 mg/s of xenon. The thruster has been widely characterised using a thrust balance, Wien filter, and a Faraday probe and results will be presented in a different publication since their discussion is outside the core of this article.

6. Conclusion

This work presents numerical and experimental studies on the design, modelling and characterisation of a novel modular hollow cathode. The modular cathode is developed to assist in ground testing

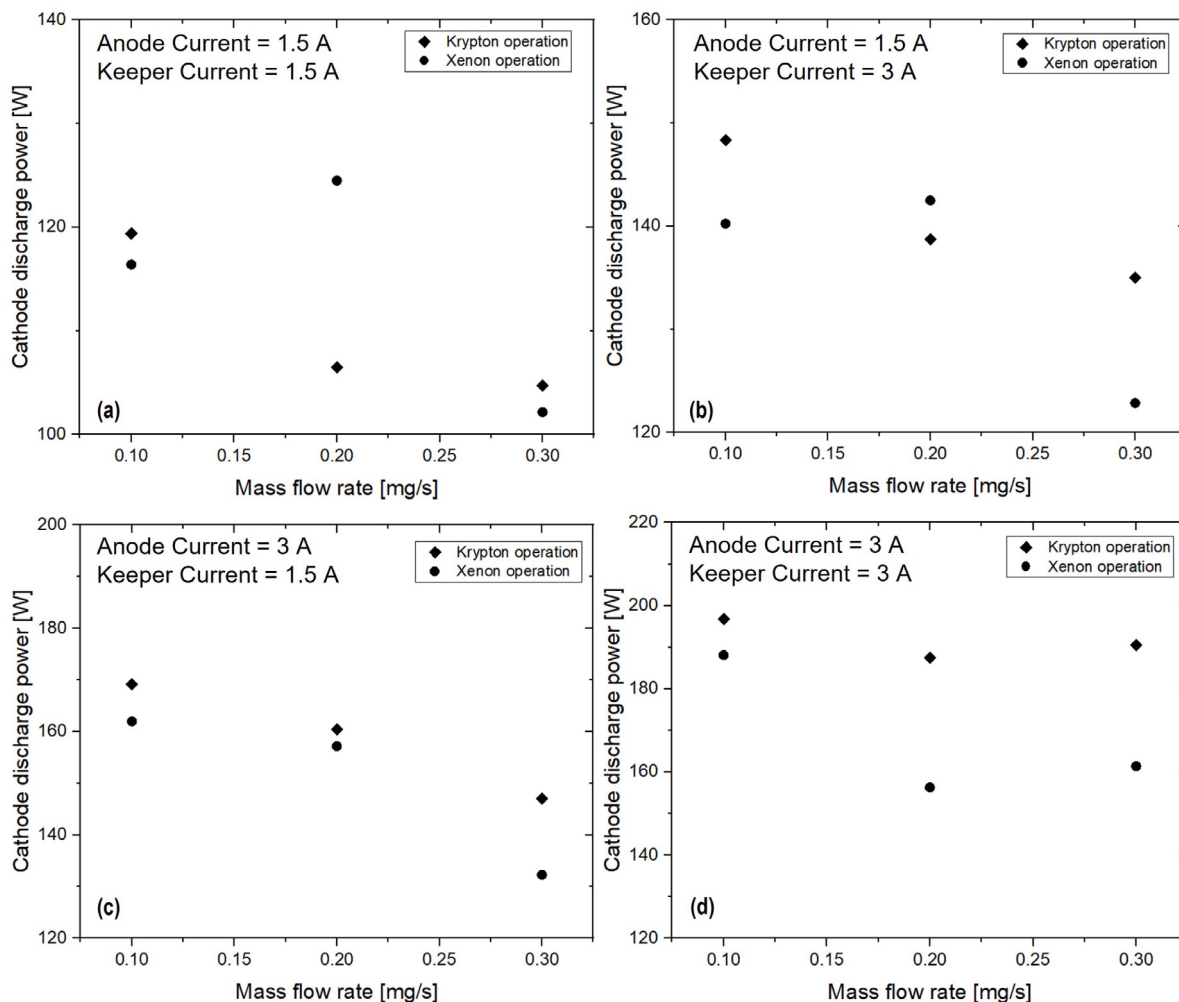


Fig. 24. Cathode discharge power as a function of the mass flow rate for the two different propellants. (a) Anode current of 1.5 A and keeper current of 1.5 A. (b) Anode current of 1.5 A and keeper current of 3 A. (c) Anode current of 3 A and keeper current of 1.5 A. (d) Anode current of 3 A and keeper current of 3 A.

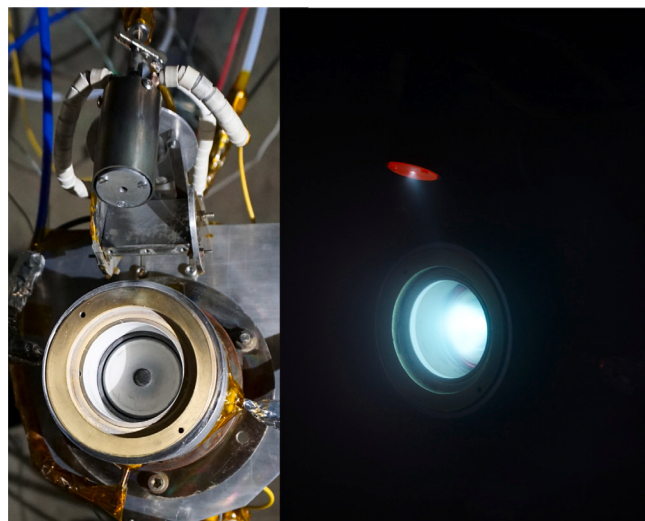


Fig. 25. Modular hollow cathode and Halo thruster set-up. On the left side the setup of the Halo thruster with the modular hollow cathode is shown. On the right side the ignition of the Halo thruster is shown.

of plasma-based thrusters at the Surrey Space Centre. The cathode's geometry introduces a new approach for heating the emitter, aiming at sustaining the heat deposition and minimising radiative heat loss. The modularity of the cathode has been introduced to ease the replacement of components in case of failure and/or to enable geometric parametric studies of the cathode. The sizing of the cathode is aided by the use of a zero-dimensional plasma model and a thermal model is also implemented using an engineering software for assisting its thermal design. The discrepancy between the measured and simulated temperatures is under < 35%.

The modular cathode's characteristics are evaluated in both standalone (diode and triode modes) and coupled operation. The cathode is tested by sweeping the keeper current from 1 to 4 A to sustain the discharge, and the collected data show that the cathode can operate at various mass flow rates in the range of 0.1 to 0.3 mg/s for xenon and krypton producing extracted currents between 0.5 A to 3.5 A. Stable operation is reached without the need for additional heater input power after ignition. The current–voltage characteristics in diode mode are compared to those predicted by the plasma model showing a good agreement between them with an offset of under 20%. The anode voltage in triode mode shows similar trends at similar keeper current and mass flow rate for both xenon and krypton. The modular hollow cathode performance on krypton replicates similar trends with respect to xenon, however on krypton the required discharge power is higher. The modular hollow cathode is successfully coupled with a non-conventional Hall-effect thruster and demonstrates stable operation

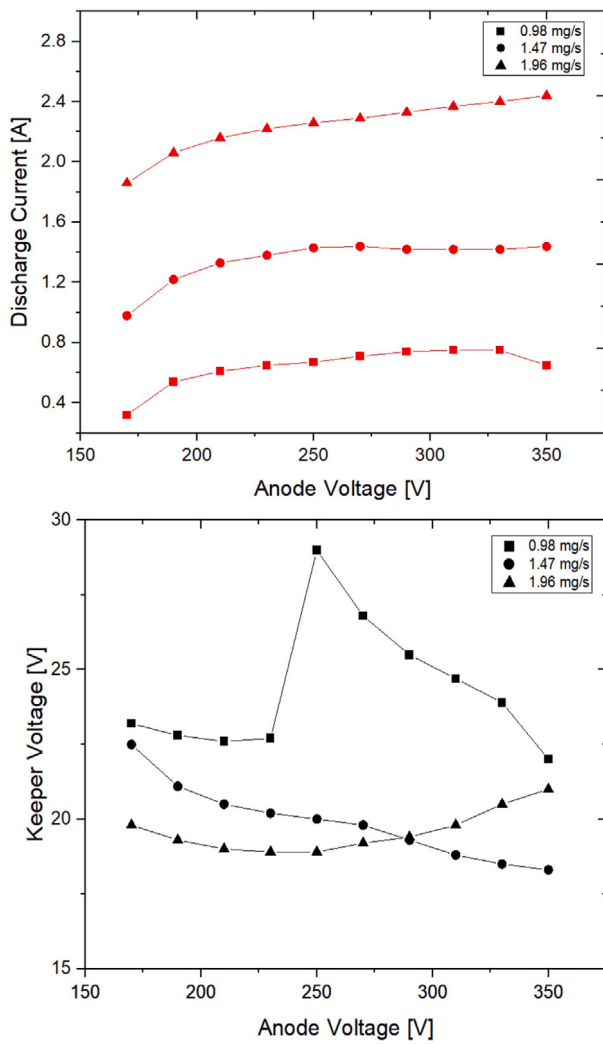


Fig. 26. Modular hollow cathode-thruster experimental operation: Anode voltage against discharge current (top) and keeper voltage (bottom) at different thruster anode mass flow rates.

providing a current between 0.3 and 2.5 A using a mass flow rate of 0.1 mg/s. As a result, it can be concluded that the modular hollow cathode is a suitable electron source for ground testing plasma thrusters.

CRediT authorship contribution statement

Mohamed Ahmed: Writing – original draft, Software, Methodology, Investigation, Formal analysis, Conceptualization. **Burak Karadag:** Writing – original draft, Validation, Software, Methodology, Investigation, Conceptualization (Initial). **Silvia Masillo:** Writing – review & editing, Methodology, Investigation, Conceptualization. **Andrea Lucca Fabris:** Writing – review & editing, Validation, Supervision, Resources, Project administration, Funding acquisition.

Declaration of competing interest

The authors declare that they have no known competing financial interests or personal relationships that could have appeared to influence the work reported in this paper.

Data availability

Data will be made available on request.

References

- [1] D. Lev, I. Mikellides, D. Pedrini, D. Goebel, B. Jorns, M. McDonald, Recent progress in research and development of hollow cathodes for electric propulsion, *Rev. Mod. Plasma Phys.* 3 (2019) <http://dx.doi.org/10.1007/s41614-019-0026-0>.
- [2] A. Gurciullo, A.L. Fabris, T. Potterton, Numerical study of a hollow cathode neutraliser by means of a zero-dimensional plasma model, *Acta Astronaut.* 174 (2020) 219–235, <http://dx.doi.org/10.1016/j.actaastro.2020.05.006>.
- [3] Starlink, Space explored, 2021, URL <https://spaceexplored.com/guides/starlink/>.
- [4] Arianespace sets a new mark; more than half of the OneWeb constellation now successfully deployed, Arianespace, 2021, URL <https://www.arianespace.com/press-release/soyuz-st36-oneweb-success/>.
- [5] T.F. Munro-O'Brien, C. Ryan, Performance of a low power Hall effect thruster with several gaseous propellants, *Acta Astronaut.* 206 (2023) 257–273, <http://dx.doi.org/10.1016/j.actaastro.2023.01.033>.
- [6] M. Nakles, W. Hargus, J. Delgado, R. Corey, A performance comparison of xenon and krypton propellant on an SPT-100 hall thruster, in: *Proceedings of 32nd International Electric Propulsion Conference*, 2011.
- [7] J.A. Linnell, A.D. Gallimore, Efficiency analysis of a hall thruster operating with krypton and xenon, *J. Propuls. Power* 22 (6) (2006) 1402–1418, <http://dx.doi.org/10.2514/1.19613>.
- [8] G.-C. Potrivitu, L. Xu, S. Huang, M.W.A. Rohaizat, S. Xu, Discharge mode transition in a Krypton-fed 1 A-class LaB6 cathode for low-power Hall thrusters for small satellites, *J. Appl. Phys.* 127 (2020) 064501, <http://dx.doi.org/10.1063/1.5142019>.
- [9] J.J. Szabo, R. Tedrake, G. Kolencik, B. Pote, Measurements of a krypton fed 1.5 kW hall effect thruster with a centrally located cathode, in: *Proceedings of 35th International Electric Propulsion Conference*, 2017.
- [10] S.B. Gabriel, A. Daykin-Iliopoulos, M. Praeger, M. Coletti, IEPC-2017-440 hollow cathode operation with different gases, in: *Proceedings of 35th International Electric Propulsion Conference*, 2017.
- [11] D. Pedrini, T. Misuri, F. Paganucci, M. Andrenucci, Development of hollow cathodes for space electric propulsion at sitael, *Aerospace* 4 (2017) 26, <http://dx.doi.org/10.3390/aerospace4020026>.
- [12] J.W.M. Lim, I. Levchenko, S. Huang, L. Xu, R.Z.W. Sim, J.S. Yee, G.-C. Potrivitu, Y. Sun, K. Bazaka, X. Wen, J. Gao, S. Xu, Plasma parameters and discharge characteristics of lab-based krypton-propelled miniaturized Hall thruster, *Plasma Sources. Sci. Technol.* 28 (6) (2019) 064003, <http://dx.doi.org/10.1088/1361-6595/ab07db>.
- [13] D.M. Goebel, K.K. Jameson, R.R. Hofer, Hall thruster cathode flow impact on coupling voltage and cathode life, *J. Propuls. Power* 28 (2) (2012) 355–363, <http://dx.doi.org/10.2514/1.B34275>.
- [14] S. Masillo, Experimental Characterisation of a Novel Hall-Type Plasma Thruster for Small Satellite Applications (Ph.D. thesis), University of Surrey, 2023.
- [15] S. Masillo, A. Fabris, T. Potterton, A. Knoll, P. Bianco, Plasma diagnostics and thrust performances of the HALO thruster with permanent magnets, in: *Proceedings of 73rd International Astronautical Congress*, 2022.
- [16] S. Masillo, A. Fabris, B. Karadag, T. Potterton, A. Knoll, P. Bianco, Experimental characterisation of the novel HALO plasma thruster for small satellite applications, in: *Proceedings of 8th Space Propulsion Conference*, 2021.
- [17] B. Karadag, S. Masillo, R. Moloney, A. Fabris, T. Potterton, A. Knoll, P. Bianco, Experimental investigation and performance optimization of the halo thruster, in: *Proceedings of 36th International Electric Propulsion Conference*, 2019.
- [18] A. Fabris, T. Wantock, A. Gurciullo, R. Moloney, A. Knoll, T. Potterton, P. Bianco, Overview of halo thruster research and development activities, in: *Proceedings of 7th SPACE PROPULSION Conference*, 2018.
- [19] R. Hofer, L. Johnson, D. Goebel, R. Wirz, Effects of internally mounted cathodes on hall thruster plume properties, *IEEE Trans. Plasma Sci.* 36 (2008) 2004–2014, <http://dx.doi.org/10.1109/TPS.2008.2000962>.
- [20] D.M. Goebel, I. Katz, *Fundamentals of Electric Propulsion: Ion and Hall Thrusters*, first ed., Wiley, 2008.
- [21] M. Domonkos, M. Patterson, A. Gallimore, Low-current, xenon orificed hollow cathode performance for in-space applications, *J. Propuls. Power* 19 (3) (2002) 438–443, <http://dx.doi.org/10.2514/2.6127>.
- [22] G.-C. Potrivitu, L. Xu, S. Xu, A low-current LaB6 open-end knife-edge emitter hollow cathode for Hall thrusters, *Plasma Sources. Sci. Technol.* 30 (2021) 085012, <http://dx.doi.org/10.1088/1361-6595/ac1b34>.
- [23] D.G. Courtney, Development and Characterization of a Diverging Cusped Field Thruster and a Lanthanum Hexaboride Hollow Cathode (M.Sc. Thesis), 2008.
- [24] V.J. Friedly, P.J. Wilbur, High current hollow cathode phenomena, *J. Propuls. Power* 8 (3) (1992) 635–643, <http://dx.doi.org/10.2514/3.23526>.
- [25] T. Meng, Z. Ning, D. Yu, Triggering of ionization oscillations in hollow cathode discharge by keeper electrode, *Phys. Plasmas* 26 (2019) 093510, <http://dx.doi.org/10.1063/1.5116830>.
- [26] D. Pedrini, C. Ducci, U. Cesari, T. Misuri, M. Andrenucci, SITAE HC1 low-current hollow cathode, *Aerospace* 7 (7) (2020) <http://dx.doi.org/10.3390/aerospace7070096>.
- [27] U. Kokal, N. Turan, M. Celik, H. Kurt, Thermal analysis and testing of different designs of lanthanum hexaboride hollow cathodes, in: *Proceedings of 8th International Conference on Recent Advances in Space Technologies*, 2017.

- [28] A. Bohnert, Thermal Characterization of a Hall Effect Thruster (Master Thesis), 2008.
- [29] U. Kokal, N. Turan, M. Celik, Thermal analysis and testing of different designs of lanthanum hexaboride hollow cathodes, MDPI- Aerospace 8 (2021) <http://dx.doi.org/10.3390/aerospace8080215>.
- [30] M. Coletti, S.B. Gabriel, Barium oxide depletion from hollow-cathode inserts: Modeling and comparison with experiments, J. Propuls. Power 26 (2) (2010) 364–369, <http://dx.doi.org/10.2514/1.41345>.
- [31] D. Pedrini, R. Albertoni, F. Paganucci, M. Andrenucci, Theoretical model of a lanthanum hexaboride hollow cathode, IEEE Trans. Plasma Sci. 43 (1) (2015) 209–217, <http://dx.doi.org/10.1109/TPS.2014.2367815>.
- [32] R. Albertoni, D. Pedrini, F. Paganucci, M. Andrenucci, A reduced-order model for thermionic hollow cathodes, IEEE Trans. Plasma Sci. 41 (7) (2013) 1731–1745, <http://dx.doi.org/10.1109/TPS.2013.2266512>.
- [33] G.-C. Potrivitu, S. Xu, Phenomenological plasma model for open-end emitter with orificed keeper hollow cathodes, Acta Astronaut. 191 (2022) 293–316, <http://dx.doi.org/10.1016/j.actaastro.2021.11.005>.
- [34] J.L. Cronin, Modern dispenser cathodes, in: IEE Proceedings, Vol. 128, 1981, <http://dx.doi.org/10.1049/ip-i-1.1981.0012>.
- [35] J.G. Andrews, J.E. Allen, D.W. Holder, Theory of a double sheath between two plasmas, Proc. R. Soc. Lond. Ser. A Math. Phys. Eng. Sci. 320 (1543) (1971) 459–472, <http://dx.doi.org/10.1098/rspa.1971.0003>.
- [36] A. Gurciullo, A. Fabris, T. Potterton, Zero-dimensional plasma model and numerical investigation of a hollow cathode neutraliser, in: Proceedings of 36th International Electric Propulsion Conference, 2019.
- [37] R. Albertoni, M. Andrenucci, D. Pedrini, F. Paganucci, Preliminary characterization of a LaB₆ hollow cathode for low-power hall effect thrusters, in: Proceedings of 33rd International Electric Propulsion Conference, 2013.
- [38] P. Guerrero, I.G. Mikellides, J.E. Polk, R. Carmina Montreal, D.I. Meiron, Critical implications of ion-surface energy accommodation and neutralization mechanism in hollow cathode physics, J. Appl. Phys. 130 (4) (2021) 043306, <http://dx.doi.org/10.1063/5.0055824>.
- [39] I. Mikellides, A. Lopez Ortega, D. Goebel, G. Becatti, Dynamics of a hollow cathode discharge in the frequency range of 1–500 kHz, Plasma Sources. Sci. Technol. 29 (2020) <http://dx.doi.org/10.1088/1361-6595/ab69e4>.
- [40] G.-C. Potrivitu, R. Jousset, S. Mazouffre, Anode position influence on discharge modes of a LaB₆ cathode in diode configuration, Vacuum 151 (2018) 122–132, <http://dx.doi.org/10.1016/j.vacuum.2018.02.010>.
- [41] I.G. Mikellides, P. Guerrero, A. Lopez Ortega, J.E. Polk, Spot-to-plume mode transition investigations in the HERME5 hollow cathode discharge using coupled 2-D axisymmetric plasma-thermal simulations, in: Joint Propulsion Conference, 2018, <http://dx.doi.org/10.2514/6.2018-4722>.
- [42] Y. Oshio, K. Kubota, H. Watanabe, S. Cho, Y. Ohkawa, I. Funaki, Experimental investigation of LaB₆ hollow cathode with radiative heater, JSASS Aerosp. Tech. 17 (2019) 203–210, <http://dx.doi.org/10.2322/tastj.17.203>.
- [43] J. Sommerville, L. King, Effect of cathode position on hall-effect thruster performance and cathode coupling voltage, in: 43rd AIAA/ASME/SAE/ASEE Joint Propulsion Conference & Exhibit, 2007, <http://dx.doi.org/10.2514/6.2007-5174>.
- [44] M. Walker, A. Gallimore, Hall thruster cluster operation with a shared cathode, J. Propuls. Power 23 (2007) 528–536, <http://dx.doi.org/10.2514/1.23688>.
- [45] Y. Raitses, E. Granstedt, A. Smirnov, E. Merino, N. Fisch, Effects of cathode electron emission on hall thruster discharge, in: 44th AIAA/ASME/SAE/ASEE Joint Propulsion Conference and Exhibit, 2008, <http://dx.doi.org/10.2514/6.2008-5188>.